Differential Scanning Calorimetry of Copolymer of Isotactic Polypropylene Backbone with Grafted Poly(ethylene-*co*-propylene) Branches

Philip M. Whitney,[1] Shiping Zhu[1,2]

[1]*Department of Chemical Engineering, McMaster University, Hamilton, Ontario, Canada L8S 4L7*
[2]*Department of Materials Science and Engineering, McMaster University, Hamilton, Ontario, Canada L8S 4L7*

Received 20 April 2005; accepted 27 August 2005
DOI 10.1002/app.23046
Published online in Wiley InterScience (www.interscience.wiley.com).

ABSTRACT: A series of graft polymers having polypropylene (PP) backbone and poly(ethylene-*co*-propylene) (EPR) side chains was prepared. PP backbone molecular weight (M_n) was 28–98 kg/mol, EPR side chain M_n was 2.6–17 kg/mol, and EPR content was 0–16 wt %. In this work, thermal analysis of the copolymers was performed using differential scanning calorimetry (DSC). Nonisothermal crystallization was performed at different cooling rates. The DSC thermograms revealed multiple melting peaks for slowly cooled samples, most likely the result of the melting of thinner tangential lamellae followed by the melting of thicker radial lamellae. Equilibrium melting temperature (T_m^0) was determined using the linear Hoffman–Weeks method. Another approach was also used for determining T_m^0: melting temperature (T_m) and crystallization temperature (T_c) were plotted as functions of logarithmic cooling rate. Linear relationships were observed for all samples with the cross points as T_m^0's. As cooling rate decreased, T_c, T_m, and enthalpy of fusion (ΔH_f) increased. T_m and T_m^0 increased with increasing PP M_n. T_c and T_m were unaffected by the grafting of EPR onto the PP backbone. T_m^0 and ΔH_f decreased as EPR content increased. © 2006 Wiley Periodicals, Inc. J Appl Polym Sci 99: 3380–3388, 2006

Key words: poly(propylene), (PP); poly(ethylene-*co*-propylene), (EPR); differential scanning calorimetry, (DSC); crystallization; melting

INTRODUCTION

Polypropylene (PP) is an important commercial plastic, but it has poor low-temperature impact strength. Today, PP is toughened by blending it with olefin elastomers, such as ethylene–propylene rubber (EPR) or ethylene–propylene–diene monomer (EPDM). The blend of olefin elastomers and PP is incompatible and forms a multiphase system. When the rubber content is below about 30 vol %, a PP matrix with dispersed rubbery domains results.

High-impact PP has high stiffness and is a good electrical insulator. It is primarily used in durable applications, such as automotive parts, including bumpers and body panels and appliances. Impact-modified PP exhibits significantly higher fracture resistance, impact strength, elongation-at-break, and fracture toughness than unmodified PP. However, modified PP has reduced modulus, tensile strength, and transparency. These properties are influenced by interfacial adhesion, the concentration of rubber, and the size, shape, and dispersion of the domains.

Correspondence to: S. Zhu (zhuship@mcmaster.ca).

Journal of Applied Polymer Science, Vol. 99, 3380–3388 (2006)

For multiphase polymers, toughening is determined by two factors.[1] First, it has been shown that the smaller the particle and the narrower the particle size distribution, the better the impact properties. Smaller particles and narrower particle size distributions partially result from low surface tension between the particle and the matrix (i.e., good compatibility between phases). Second, it has been demonstrated that the stronger the adhesion between the particle and the matrix, the better the impact properties. Strong interfacial adhesion is also the result of good compatibility.

Nitta, Mori, and coworkers synthesized diblock copolymers of isotactic PP and ethylene–propylene random copolymer (PP-*b*-EPR) by a short-period (or stopped-flow) polymerization method.[2–8] They used differential scanning calorimetry (DSC) for thermal analysis of the PP-*b*-EPR, along with a PP homopolymer and a PP/EPR blend.[4] The PP and PP/EPR blend had the same melting temperature (T_m) of 157°C. T_m decreased with increasing EPR fraction in the PP-*b*-EPR, from 157 to 147°C. A similar trend was reported in other papers by the same group.[2,7]

Wang and Huang reported the synthesis of PP-EPR and PP-EPR-PP block copolymers by sequential slurry polymerization with δ-$TiCl_3$-Et_2AlCl in hexane.[9] DSC of the PP-EPR and PP-EPR-PP copolymers revealed two melting endotherms, one at 154–162°C, attribut-

able to PP, and the other at 119–121°C, attributable to long ethylene sequences in the EPR block.[9] Similarly, there were two crystallization peaks, one for PP and one for PE.

Arranz-Andrés et al. studied a commercially available propylene-*b*-(ethylene-*co*-propylene) copolymer, which is composed of iPP and EPR units.[10,11] The copolymer was supplied by Repsol-YPF (Spain). It was synthesized as follows: An iPP homopolymer was produced in a first reactor, and then propylene and ethylene were fed in a second reactor. This resulted in a multiphasic copolymer composed of blocks of semicrystalline iPP and amorphous EPR. DSC analysis was performed on this PP-*b*-EPR.[10] The copolymer was quenched from the melt and then heated at 20°C/min, revealing two peaks upon melting. The existence of two peaks was attributed to a melting–recrystallization–melting process acting on imperfect crystallite formation.

Lohse and coworkers prepared a graft copolymer with iPP arms pendant from an EPR backbone and demonstrated its ability to compatibilize iPP/EPR blends.[12,13] In the first step, an ethylene–propylene–diene terpolymer (EPDM) was made.[12] In the second step, iPP chains were grown from the unreacted double bonds of the diene. Alternatively, a succinic anhydride grafted PP was reacted with an EPR containing primary amine groups.[13]

Ruokolainen et al. synthesized a syndiotactic PP-*b*-EPR using a bis(phenoxyimine)-based titanium catalyst system with methylaluminoxane.[14] The reactor was first saturated with propylene and then injected with the catalyst to initiate polymerization. After some time, the reactor was vented and ethylene was introduced into the reactor. After additional time, the reaction was quenched. Using DSC, T_c and T_m were discovered to correlate best with the sPP-EPR block copolymer total molecular weight, with higher molecular weights producing lower T_c and T_m.

Coates and coworkers have also synthesized a syndiotactic PP-*b*-EPR.[15,16] T_m decreased with the addition of EPR. Fukui and Murata synthesized an atactic PP-*b*-EPR using metallocene catalyst systems.[17]

Recently, Kolodka et al. synthesized a series of novel polymers with iPP backbones and EPR branches.[18,19] The molecular weight of EPR side chains and the EPR weight percentage in the copolymer were well controlled. There appeared to be a critical EPR branch length at an M_n of about 6 or 7 kg/mol. When the EPR length was below this M_n, the side chains behaved as short chain branches and had little influence on rheological properties. If this critical M_n was exceeded, the side chains were long enough to form entanglements and behaved as long chain branches. Increasing branch M_n and branch frequency led to increases in zero shear viscosity, shear thinning, and flow activation energy. A two-phase system also developed, with fine rubbery domains dispersed in a PP matrix. The two-phase system enhanced the loss modulus of the copolymer. The domain sizes depended on the M_n of individual EPR branches, and were nanoscale. Because the EPR chains were chemically grafted to the PP backbone, there was excellent dispersion of rubbery domains.

The objective of the present work is to establish the relationships between chain structure (i.e., PP M_n, EPR content, and EPR M_n) and thermal properties (i.e., crystallization and melting behavior) using the polymers synthesized by Kolodka et al. Thermal analysis of the polymers is performed using DSC.

EXPERIMENTAL

Synthesis of PP-*g*-EPR

The copolymers of iPP and EPR used in this work were synthesized in a two-step polymerization process. First, EPR macromonomers were prepared in a high-temperature, high-pressure continuous stirred tank reactor using a Dow Chemical constrained geometry catalyst, $[C_5Me_4(SiMe_2N^tBu)]TiMe_2$ with cocatalyst, tris(pentafluorophenyl)boron. The details regarding the reactor system and the polymerization were reported in previous publications.[20,21] Next, the EPR macromonomers were copolymerized with propylene in a semibatch reactor using *rac*-dimethylsilylenebis(2-methylbenz[e]indenyl) zirconium dichloride and modified methyl aluminoxane.

Differential scanning calorimetry

The heating, cooling, and heat measurements of polymer samples were performed using a TA Instruments DSC 2910 Modulated DSC. The DSC was operated in Conventional DSC mode for all experiments. The DSC was connected to a TA Instruments DSC Refrigerated Cooling System. The DSC was controlled using Thermal Advantage Instrument Control Software.

A nitrogen purge rate of 30 mL/min was used for all experiments. The DSC cell constant and temperature were calibrated using indium. Polymer samples weighed about 5–10 mg, and were crimped in aluminum pans.

Samples were heated at 10°C/min to 180–210°C and held there for 10 min to erase thermal history. They were then cooled at different rates (0.2 or 0.3, 1, 3, and 10°C/min) to 50–80°C. Crystallization temperature (T_c) was measured during cooling. The slowest cooling rate was 0.2°C/min for samples 1, 6, 7, and 13 (and 0.3°C/min for all others). Cooling was followed by a second heating scan at 10°C/min. Melting temperature (T_m) and enthalpy of fusion (ΔH_f) were measured during the second heating scan.

TABLE I
Crystallization Results From DSC

Sample	PP M_n (kg/mol)	EPR M_n (kg/mol)	EPR content (wt %)	EPR branch per PP chain	T_c (°C)			
					10°C/min	3°C/min	1°C/min	0.2 or 0.3°C/min
1	54.5	2.6	7.6	1.75	115.3	118.9	123.0	128.0
2	52.8	3.9	10.7	1.62	113.0	119.0	123.3	127.7
3	50.1	6.0	8.6	0.78	113.1	117.8	121.7	126.1
4	34.6	7.8	15.7	0.82	111.0	116.7	121.2	125.6
5	34.4	11.2	16.1	0.59	115.8	121.2	125.4	130.0
6	90.4	17.1	8.7	0.50	115.8	120.8	125.1	130.9
7	97.7	0.0	0.0	0.00	116.3	120.1	123.9	129.9
8	51.7	2.6	2.4	0.50	112.0	117.8	122.2	126.4
9	52.7	2.6	4.5	0.97	118.8	122.5	125.4	128.9
10	45.7	2.6	5.4	1.02	111.3	117.8	122.6	127.2
11	74.0	17.1	1.4	0.06	112.0	116.8	121.6	125.7
12	77.4	17.1	3.3	0.15	115.0	120.4	124.6	128.6
13	30.0	2.6	5.3	0.66	108.3	113.9	118.5	124.5
14	28.1	2.6	4.5	0.52	115.6	119.5	122.5	125.7

RESULTS AND DISCUSSION

The results of crystallization and melting are summarized in Tables I and II, respectively. The data on molecular weight (M_n) and EPR content are from the previous work.[19] The reported T_c is the temperature at which crystallization commenced (i.e., onset of crystallization). The reported T_m is the peak T_m. After rapid cooling, there was only one melting peak upon heating. The T_m's reported for the slow cooling experiments are of the dominant peak, in the cases where there are low temperature shoulders or peaks.

Multiple melting peaks

After the polymer samples were cooled rapidly (10°C/min), only one endothermic peak was visible upon melting. Slower cooling led to the development of an endothermic melting shoulder at a temperature about 10°C lower than the main melting peak. Further decreasing the cooling rate allowed the shoulder to develop into a more well-defined melting peak (Fig. 1). This phenomenon is evident for all the polymer samples tested. There is no significant difference between the melting peaks of samples 6 and 7 at any cooling rate, despite the presence of EPR in sample 6 (Figs. 2–4).

Many different explanations have been given for the presence of multiple melting peaks in the DSC thermograms of iPP. Explanations vary based on the polymer chain structure and the crystallization conditions. One explanation is the formation of different crystalline polymorphs (α-, β-, or γ-forms), which have dif-

TABLE II
Melting Results From DSC

Sample	T_m (°C)				ΔH_f (J/g)			
	10°C/min	3°C/min	1°C/min	0.2 or 0.3°C/min	10°C/min	3°C/min	1°C/min	0.2 or 0.3°C/min
1	147.2	148.0	149.4	150.8	92	95	96	96
2	148.2	149.0	150.2	151.6	95	97	103	103
3	147.9	148.7	149.8	151.1	98	99	98	105
4	148.0	148.5	149.6	150.6	87	97	98	104
5	149.5	150.2	151.1	152.7	91	95	100	100
6	151.9	152.8	154.1	156.1	88	92	94	97
7	151.3	151.9	153.5	156.3	102	105	110	116
8	146.9	147.9	149.3	150.6	113	115	118	122
9	148.9	149.6	150.6	151.6	98	105	109	111
10	143.2	144.6	147.0	148.1	108	106	117	115
11	149.1	150.2	151.6	153.6	101	106	110	115
12	149.3	150.2	151.9	152.5	74	77	81	90
13	142.1	143.1	144.8	146.3	95	100	99	99
14	144.6	144.9	146.1	147.0	102	105	113	110

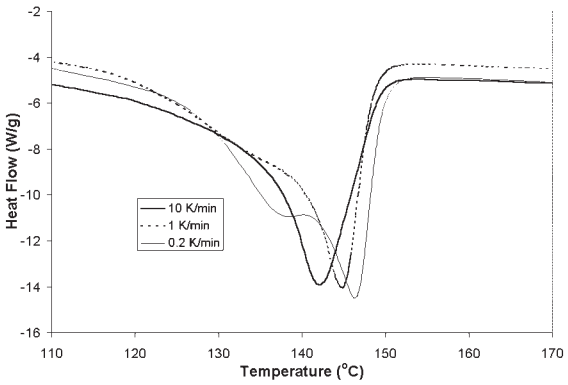

Figure 1 DSC melting curves for sample 13 after cooling at 0.2, 1, and 10°C/min.

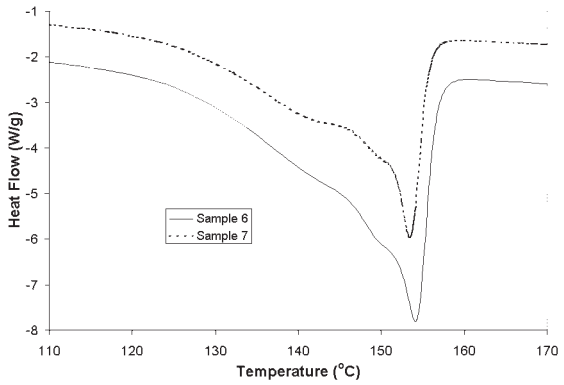

Figure 3 DSC melting curves for samples 6 and 7 after cooling at 1°C/min.

ferent T_m's. In cases where both α- and β-forms are present, the two melting peaks represent the melting of α- and β-crystals, where the β-crystals melt at a lower temperature.[22–25] For isothermal crystallization, the relative content of the β-form decreases with increasing T_c.[24] For nonisothermal crystallization, the percent of β-form decreases when cooling rate decreases.[23] These results from isothermal and nonisothermal experiments are consistent, because slower cooling results in higher T_c. This explanation will not work for the results found in the present research, because the intensity of the lower peak increases with slower cooling.

Another possibility involving two crystal forms is that the two peaks represent the α- and γ-crystals, where the γ-crystals melt at a lower temperature.[26–28] The γ-phase of iPP can be formed by using high pressures during crystallization. It can also be formed at atmospheric pressure in homoPP with a high concentration of stereodefects and regiodefects in the chain and in PP copolymers. The percent of γ-phase increases with decreasing cooling rate or increasing isothermal T_c.[28–31] Therefore, the double melting peaks are more prominent after slow cooling. This is the same trend observed in the present research. However, γ-crystals are not the only possible explanation for the multiple melting peaks observed in the present research.

The second possible explanation for the multiple melting peaks is a melting-recrystallization process that occurs during heating after crystallization. In this case, the double melting peak is not related to the structure or morphology of the original crystallized sample. Instead, the low melting peak corresponds to the partial melting of the original crystals, and the high melting peak corresponds to the melting of crystals formed during the melting process.[32] Upon heating in the DSC, thin molten lamellae recrystallize into thicker lamellae, which melt at higher temperatures. This explanation involves melting of a disordered phase α_1, followed by recrystallization into an ordered phase α_2, and finally the melting of α_2.[25,33–35]

In isothermal crystallization experiments, multiple melting peaks are produced after crystallization at a low T_c, but not at a high T_c.[35–37] Similarly, in nonisothermal crystallization experiments, many researchers have found multiple melting peaks after fast cooling (low T_c), but only one melting peak after slow cooling

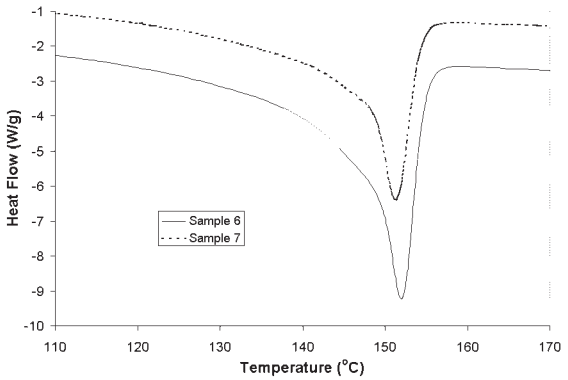

Figure 2 DSC melting curves for samples 6 and 7 after cooling at 10°C/min.

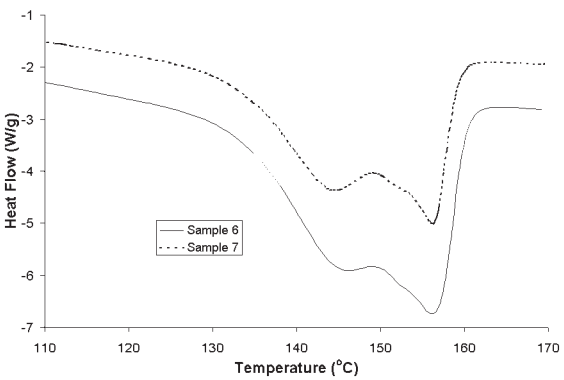

Figure 4 DSC melting curves for samples 6 and 7 after cooling at 0.2°C/min.

(high T_c).[33,37–40] Therefore, this explanation is more likely valid for low isothermal T_c or for rapid cooling, for which more imperfect crystals are formed. At lower cooling rates, greater percentages of the sample crystallize perfectly and, therefore, the percentage of polymer that undergoes reorganization decreases. Conversely, in the present research the double melting peaks are visible only after slow cooling.

A third possibility is that the two endothermic peaks correspond to the melting of two populations of lamellae. It is well-known that spherulites of iPP contain two populations of lamellae, namely the *radial* (or *dominant* or *mother*) lamellae and the *tangential* (or *subsidiary* or *daughter*) lamellae.[41,42] The tangential lamellae form a cross-hatched structure across the radial lamellae. When this is the cause of the double melting peaks, it is because the radial lamellae are thicker and therefore melt at a higher temperature than the thinner tangential lamellae, according to the Gibbs–Thomson equation (eq. (1)), which can be simplified as follows:

$$T_m = T_m^o\left(1 - \frac{2\sigma_e}{\Delta H_f^o L}\right) \tag{1}$$

where σ_e is the fold surface free energy, ΔH_f^0 is the heat of fusion of an infinitely thick crystal, and L is the lamellar thickness.

It has been demonstrated that at low T_c, radial and tangential lamellae have the same thickness.[43–45] At low T_c, the tangential lamellae develop at almost the same time as the radial lamellae, and thus they have similar thicknesses.[43] Therefore, it is expected that at low T_c the melting of radial and tangential lamellae occur simultaneously. This has been experimentally demonstrated by Alamo et al.[45] As T_c increases, the thickness increases of both radial and tangential lamellae. However, the rate of increase of radial lamellar thickness with increasing T_c is greater than the rate of increase of tangential lamellar thickness with increasing T_c.[44,45] At high T_c, the radial lamellae grow before the tangential lamellae, and thus the radial lamellae have greater thickness.[43] Therefore, after crystallization at high temperatures, upon heating, the thin tangential lamellae melt first, and then the thicker radial lamellae melt.[45–47] Weng et al. demonstrated that different lamellar thicknesses cause multiple melting in metallocene-catalyzed PP and in propylene-ethylene random copolymers.[46,48]

It has been shown that different explanations apply in different circumstances. For α-form PP, when the supercooling is high (i.e., at low T_c or fast cooling rate), double endotherms are caused by melt-recrystallization.[49,50] When the supercooling is lower (i.e., at high T_c or slow cooling rate), double endotherms are caused by multiple populations of lamellae with different thicknesses.[49–52] Intermediate supercooling results in only one melting peak. The T_c and T_m ranges, in which each explanation applies, vary based on factors such as the isotacticity and molecular weight of the PP under investigation. Zhao et al. demonstrated the applicability of these explanations to a propylene-ethylene copolymer.[53]

The explanation involving different lamellar thicknesses is in accordance with the observations of the present research. There is only one melting peak at low T_c, but there are two melting peaks at high T_c. This indicates that the experiments were conducted in the low to intermediate supercooling ranges described above. Another possibility is that the multiple peaks represent the melting of γ- and α-crystals. This explanation cannot be ruled out based on DSC measurements alone. The other explanations, involving β-crystals or melt-recrystallization, are only applicable when the opposite trend is observed (i.e., one melting peak at high T_c and two melting peaks at low T_c).

Equilibrium melting temperature

Observed T_m's of polymers are well below the thermodynamic values, even when using slow cooling and heating rates. The difference between observed T_m and $T_m{}^0$ can be minimized by increasing T_c. In the case of nonisothermal crystallization, increasing T_c can be achieved by using lower cooling rates. In both isothermal and nonisothermal experiments, higher T_c leads to the formation of thicker lamellae, which increases T_m. The dependence of T_m on lamellar thickness is described by the Gibbs–Thomson equation (eq. (1)). The longest crystallizable sequences form the thickest lamellae, which melt at the highest temperature.

Hoffman and Weeks devised a method for studying the dependence of T_m on T_c.[54] They observed that a straight line is obtained when T_m is plotted as a function of T_c. T_m^0 is the temperature where the polymer crystallizes infinitely slowly and T_m equals T_c. Therefore, the intersection of the two lines (T_m versus T_c and $T_m = T_c$) represents T_m^0 (see Fig. 5). The Hoffman–Weeks equation is:

$$T_m = T_m^o\left(1 - \frac{1}{\gamma}\right) + \frac{T_c}{\gamma} \tag{2}$$

where γ is the morphological factor or thickening coefficient, which represents the ratio between the final lamellar thickness after thickening and the initial lamellar thickness at T_c. The greater the value of γ, the more stable the crystals.

A nonlinear Hoffman–Weeks method has been developed by Xu and coworkers.[55,56] Whereas Xu et al. argue that linear Hoffman–Weeks method underestimates $T_m{}^0$ of iPP by about 27°C, Yamada et al. argue

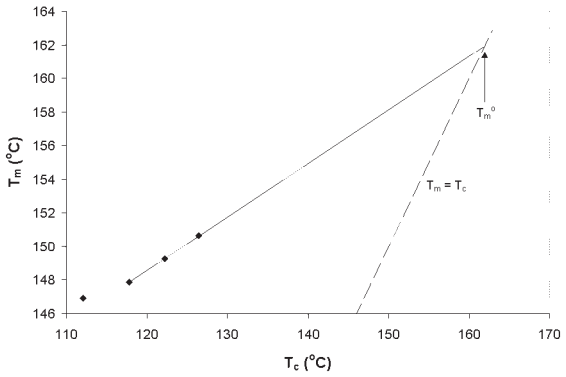

Figure 5 Hoffman–Weeks plot for determination of equilibrium melting temperature. Data shown are for sample 8.

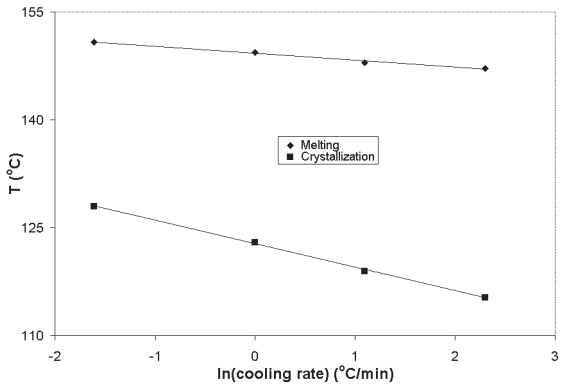

Figure 6 Effect of logarithmic cooling rate on crystallization and melting temperatures. Data shown are for sample 1.

that linear Hoffman–Weeks *over*estimates T_m^0 by about 17°C.[53,55,56] Clearly, there is still uncertainty about the true T_m^0 of iPP. The linear Hoffman–Weeks method continues to be used in the literature.[27,57]

The results of the Hoffman–Weeks extrapolations are shown in Table III. The lowest temperature has been excluded from the calculation of T_m^0, except for samples 10, 12, and 13, where no data was excluded. Excluding data from low temperatures is commonplace in the literature.[27,58,59] The slow rate of change of T_m with T_c in the low T_c region can be explained as follows.[60] Samples crystallized at low temperatures (or high cooling rates) traverse a temperature interval in which rapid crystallization occurs. Consequently, small lamellae of approximately the same thickness are formed at each T_c in this temperature range. Therefore, T_m increases very slowly with increasing T_c.

The differential coefficient ($dT_m/dT_c = 1/\gamma$) ranged between 0.24 and 0.33 for the graft copolymers and was 0.45 for the homoPP. For $T_c < 159$°C, Yamada et al. found a differential coefficient of 0.31 for their homoPP.[51] Other researchers found differential coefficients of 0.29–0.47 for various homoPPs.[37,59]

T_m and T_c as functions of cooling rate

Both T_m and T_c were plotted as functions of logarithmic cooling rate (Fig. 6). A linear relationship was observed in both cases for all samples. It was observed that these lines would intersect at very low cooling rates. The intersection of these lines gives the T_m^0. For this method, when only 3 points were used, the highest cooling rate has been excluded.

The linear relationship between T_c and logarithmic cooling rate has been observed in previous reports.[61,62] This is in contrast to the linear relationship between T_c and (nonlogarithmic) cooling rate proposed by Khanna and the related crystallization rate coefficient (CRC).[63] Since T_c is linearly correlated with logarithmic cooling rate, and T_m is linearly correlated with T_c (according to the Hoffman–Weeks equation),

TABLE III
Equilibrium Melting Temperature Results by Two Methods

	Hoffman–Weeks		ln (rate)	T_m vs. ln (rate)		T_c vs. ln (rate)	
Sample	T_m (°C)	R^2	T_m (°C)	R^2	# Points	R^2	# Points
1	161.4	0.9974	160.3	0.9884	4	0.9987	4
2	161.6	0.9999	161.7	0.9999	3	0.9997	3
3	161.3	1.0000	161.0	0.9997	3	0.9996	4
4	158.5	0.9997	158.5	0.9982	3	0.9993	3
5	161.5	0.9797	159.3	0.9612	4	1.0000	3
6	168.6	0.9983	167.8	0.9997	3	0.9986	4
7	177.5	0.9991	179.1	0.9976	3	0.9986	4
8	161.9	1.0000	159.1	0.9927	4	0.9949	4
9	161.8	0.9976	161.6	0.9993	3	0.9996	4
10	158.2	0.9747	158.3	0.9784	4	0.9939	4
11	171.0	0.9759	170.6	0.9931	3	0.9976	4
12	160.1	0.9673	161.1	0.9665	4	0.9990	3
13	154.3	0.9823	154.3	0.9860	4	0.9970	4
14	157.6	0.9912	157.6	0.9889	3	0.9999	3

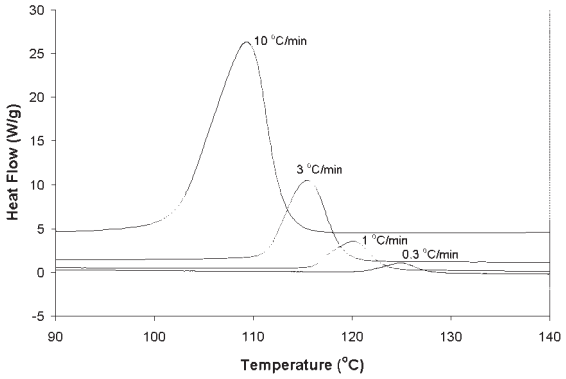

Figure 7 DSC crystallization curves for sample 2 cooled at various rates.

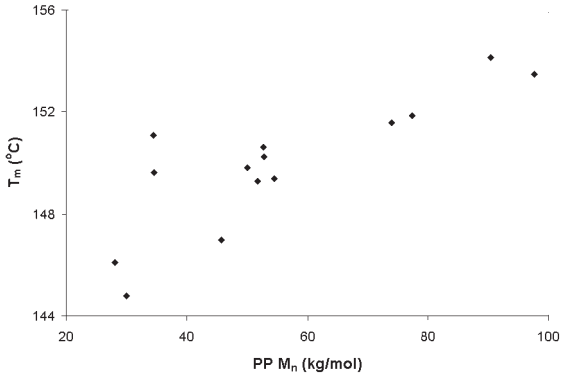

Figure 8 Effect of PP molecular weight on melting temperature (after cooling at 1°C/min).

T_m must also be linearly correlated with logarithmic cooling rate, as shown here.

Effect of cooling rate

T_c increases with decreasing cooling rate (Fig. 7). At lower cooling rates, the activation of crystallization nuclei occurs at higher temperatures because there is more time to overcome the nucleation barrier.[64] ΔH_f increases with decreasing cooling rate. Flexible polymer chains form amorphous, random-coil conformations in polymer melts. Fast cooling rates trap amorphous regions of a semicrystalline polymer and minimize the crystalline ordering that takes place upon cooling. T_m increases with decreasing cooling rate. Quickly cooled samples do not have enough time to form organized crystal structures. At low cooling rates, crystal thickening occurs, which leads to more perfect crystals due to longer times for reorganization within crystals.

Effect of PP M_n

PP M_n had no apparent effect on T_c or ΔH_f. T_m increases with increasing PP M_n (Fig. 8). This relationship has been observed by other researchers.[7,58] The implication is that higher molecular weight leads to greater lamellar thickness. T_m^0 increases with increasing PP M_n (Fig. 9). Cheng et al. found that the T_m^0 of iPP (isotacticity > 0.99) increases from 170°C at M_n = 15 kg/mol to 185°C at M_n = 300 kg/mol.[58] Yamada et al. showed that the T_m^0 of iPP ([mmmm] = 99.6%) increases with increasing M_n, from 183.7°C at 23 kg/mol to 187.7°C at 263 kg/mol.[65] See Mandelkern and Stack for discussion of this relationship.[66]

Effect of EPR content

T_c was unaffected by the grafting of EPR onto the iPP chain. In mechanical and reactor blends of iPP/EPR, the EPR domains can act as crystallization nuclei, producing more crystals, which lead to faster crystallization, thereby increasing T_c in nonisothermal crystallization experiments.[40,67,68] Since the T_c of the PP-*g*-EPR is independent of EPR content, the EPR side chains do not act as crystallization nuclei for PP.

ΔH_f decreases as percent EPR increases (Fig. 10). Experimental errors in the determination of ΔH_f from DSC measurements are fairly large (±5–10 J/g). Therefore, the general trend is significant, but individual points are not significant. This relationship has also been observed for PP/EPR blends.[69] It is due to the thickening of amorphous layers between lamellae, which is caused by the increased amorphous content of the PP-*g*-EPR. The decrease in ΔH_f is approximately proportional to the amorphous EPR fraction. The crystallization of PP is unhindered by the EPR side chains.

T_m was unaffected by the grafting of EPR onto the PP chain. The EPR in PP/EPR blends does not usually affect the T_m of the PP.[40,68,70] However, Bedia et al. reported a decrease in T_m of 2.8°C from homoPP to a 50% EPR blend.[69] The lack of change in T_m suggests that the incorporation of EPR does not affect lamellar thickness.

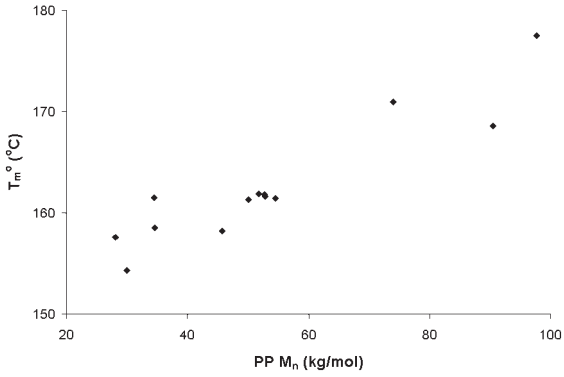

Figure 9 Effect of PP molecular weight on equilibrium melting temperature, as determined by the Hoffman–Weeks method.

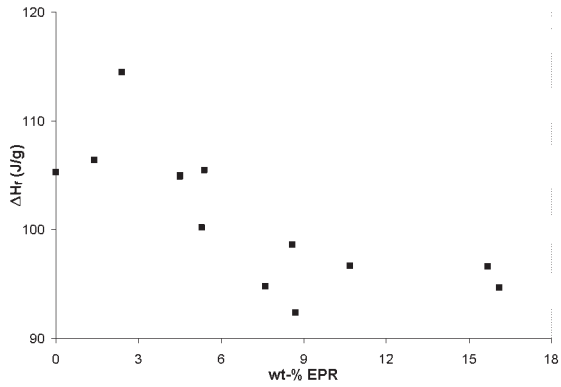

Figure 10 Effect of EPR content on enthalpy of fusion (after cooling at 3°C/min).

$T_m{}^0$ is lowered by the presence of EPR branches. The $T_m{}^0$ of the homopolymer, sample 7, is approximately 10°C higher than that of the copolymer with a similar M_n, sample 6. Furthermore, sample 11, which has a low EPR content (1.4 wt %) and a low branch frequency (0.06), has a $T_m{}^0$ higher than sample 6 and considerably higher than any of the other copolymers (Fig. 9).

Effect of EPR M_n

The length of the EPR side chains has no apparent influence on the T_c. There is no discernible influence of EPR M_n on ΔH_f. ΔH_f decreased solely as a function of EPR content, and not as a function of EPR chain length. EPR M_n does not affect experimental T_m.

EPR M_n has no effect on T_m^0. At first glance, it may appear that T_m^0 increases at the highest EPR M_n (17.1 kg/mol). However, these T_m^0s can be explained with reference to the polymer characteristics discussed in previous sections. The highest of these T_m^0s is that of sample 11. This sample has a low EPR content and a low branch frequency. The second highest T_m^0 at this EPR M_n is that of sample 6, which has the highest total M_n.

CONCLUSIONS

DSC was used to characterize unique PP-*g*-EPR samples in terms of nonisothermal crystallization and melting. The DSC thermograms revealed multiple melting peaks for slowly cooled samples, most likely the result of the melting of thinner tangential lamellae followed by the melting of thicker radial lamellae, although this cannot be proved based on DSC measurements alone. The multiple melting peaks were not the result of the presence of β-crystals (in addition to α-crystals), nor were they the result of the melting-recrystallization–remelting phenomenon.

As cooling rate decreased, T_c, ΔH_f, and T_m all increased. T_c and ΔH_f were unaffected by PP M_n. T_m and T_m^0 increased with increasing PP M_n. T_c was unaffected by the grafting of EPR onto the PP chain. ΔH_f decreased as EPR content increased. Experimental T_m was unaffected by the EPR content in the PP chain. However, T_m^0 was lowered by the EPR branches. The M_n of the EPR side chains had no apparent effect on T_c, ΔH_f, T_m, or T_m^0.

References

1. Cai, H.; Luo, X.; Chen, X.; Ma, D.; Wang, J.; Tan, H. J Appl Polym Sci 1999, 71, 103.
2. Nitta, K.; Kawada, T.; Prokhorov, V. V.; Yamahiro, M.; Mori, H.; Terano, M. J Appl Polym Sci 1999, 74, 958.
3. Nitta, K.; Kawada, T.; Yamahiro, M.; Mori, H.; Terano, M. Polymer 2000, 41, 6765.
4. Yamahiro, M.; Mori, H.; Nitta, K.-h.; Terano, M. Macromol Chem Phys 1999, 200, 134.
5. Yamahiro, M.; Mori, H.; Nitta, K.-h.; Terano, M. Polymer 1999, 40, 5265.
6. Mori, H.; Yamahiro, M.; Tashino, K.; Ohnishi, K.; Nitta, K.-h.; Terano, M. Macromol Rapid Commun 1995, 16, 247.
7. Mori, H.; Yamahiro, M.; Prokhorov, V. V.; Nitta, K.; Terano, M. Macromolecules 1999, 32, 6008.
8. Prokhorov, V. V.; Nitta, K.; Terano, M. Macromol Chem Phys 2004, 205, 179.
9. Wang, L.; Huang, B. J Polym Sci Part B: Polym Phys 1991, 29, 1447.
10. Arranz-Andrés, J.; Benavente, R.; Peña, B.; Pérez, E.; Cerrada, M. L. J Polym Sci Part B: Polym Phys 2002, 40, 1869.
11. Arranz-Andrés, J.; Benavente, R.; Pérez, E.; Cerrada, M. L. Polym J 2003, 35, 766.
12. Datta, S.; Lohse, D. J. Macromolecules 1993, 26, 2064.
13. Lohse, D. J.; Datta, S.; Kresge, E. N. Macromolecules 1991, 24, 561.
14. Ruokolainen, J.; Mezzenga, R.; Fredrickson, G. H.; Kramer, E. J.; Hustad, P. D.; Coates, G. W. Macromolecules 2005, 38, 851.
15. Radulescu, A.; Mathers, R. T.; Coates, G. W.; Richter, D.; Fetters, L. J. Macromolecules 2004, 37, 6962.
16. Tian, J.; Hustad, P. D.; Coates, G. W. J Am Chem Soc 2001, 123, 5134.
17. Fukui, Y.; Murata, M. Appl Catal A 2002, 237, 1.
18. Kolodka, E.; Wang, W.-J.; Zhu, S.; Hamielec, A. E. Macromol Rapid Commun 2002, 23, 470.
19. Kolodka, E.; Wang, W.-J.; Zhu, S.; Hamielec, A. E. Macromolecules 2002, 35, 10062.
20. Park, S.; Wang, W.-J.; Zhu, S. Macromol Chem Phys 2000, 201, 2203.
21. Wang, W.-J.; Kolodka, E.; Zhu, S.; Hamielec, A. E. J Polym Sci Part A: Polym Chem 1999, 37, 2949.
22. Aboulfaraj, M.; Ulrich, B.; Dahoun, A.; G'Sell, C. Polymer 1993, 34, 4817.
23. Fan-Chiang, C. C.; Chiu, W. Y.; Hsieh, K. H.; Chen, L. W. Mater Chem Phys 1993, 34, 52.
24. Marigo, A.; Marega, C.; Causin, V.; Ferrari, P. J Appl Polym Sci 2004, 91, 1008.
25. Yuan, Q.; Jiang, W.; An, L. Colloid Polym Sci 2004, 282, 1236.
26. Bond, E. B.; Spruiell, J. E.; Lin, J. S. J Polym Sci Part B: Polym Phys 1999, 37, 3050.
27. Xu, J.-T.; Guan, F.-X.; Yasin, T.; Fan, Z. -Q. J Appl Polym Sci 2003, 90, 3215.
28. Hosier, I. L.; Alamo, R. G.; Esteso, P.; Isasi, J. R.; Mandelkern, L. Macromolecules 2003, 36, 5623.

29. Mezghani, K.; Phillips, P. J. Polymer 1998, 39, 3735.
30. Foresta, T.; Piccarolo, S.; Goldbeck-Wood, G. Polymer 2001, 42, 1167.
31. Dai, P. S.; Cebe, P.; Capel, M. J Polym Sci Part B: Polym Phys 2002, 40, 1644.
32. Petraccone, V.; Guerra, G.; De Rosa, C.; Tuzi, A. Macromolecules 1985, 18, 813.
33. Paukkeri, R.; Lehtinen, A. Polymer 1993, 34, 4083.
34. Naiki, M.; Kikkawa, T.; Endo, Y.; Nozaki, K.; Yamamoto, T.; Hara, T. Polymer 2000, 42, 5471.
35. Celli, A.; Fichera, A.; Marega, C.; Marigo, A.; Paganetto, G.; Zannetti, R. Eur Polym J 1993, 29, 1037.
36. Tiganis, B. E.; Shanks, R. A.; Long, Y. J Appl Polym Sci 1996, 59, 663.
37. Bogoeva-Gaceva, G.; Janevski, A.; Grozdanov, A. J Appl Polym Sci 1998, 67, 395.
38. Feng, Y.; Jin, X.; Hay, J. N. Polym J 1998, 30, 215.
39. Zhu, X.; Li, Y.; Yan, D.; Zhu, P.; Lu, Q. Colloid Polym Sci 2001, 279, 292.
40. Zheng, Q.; Lin, Z.; Peng, M. Polym Int 2004, 53, 1087.
41. Bassett, D. C.; Olley, R. H. Polymer 1984, 25, 935.
42. Norton, D. R.; Keller, A. Polymer 1985, 26, 704.
43. Janimak, J. J.; Cheng, S. Z. D.; Giusti, P. A.; Hsieh, E. T. Macromolecules 1991, 24, 2253.
44. White, H. M.; Bassett, D. C. Polymer 1997, 38, 5515.
45. Alamo, R. G.; Brown, G. M.; Mandelkern, L.; Lehtinen, A.; Paukkeri, R. Polymer 1999, 40, 3933.
46. Weng, J.; Olley, R. H.; Bassett, D. C.; Jääskeläinen, P. J Macromol Sci: Phys 2002, B41, 891.
47. Weng, J.; Olley, R. H.; Bassett, D. C.; Jääskeläinen, P. J Polym Sci Part B: Polym Phys 2003, 41, 2342.
48. Weng, J.; Olley, R. H.; Bassett, D. C.; Jääskeläinen, P. J Polym Sci Part B: Polym Phys 2004, 42, 3318.
49. Janimak, J. J.; Cheng, S. Z. D.; Zhang, A.; Hsieh, E. T. Polymer 1992, 33, 728.
50. Zhu, X.; Yan, D.; Tan, S.; Wang, T.; Yan, D.; Zhou, E. J Appl Polym Sci 2000, 77, 163.
51. Yamada, K.; Hikosaka, M.; Toda, A.; Yamazaki, S.; Tagashira, K. Macromolecules 2003, 36, 4790.
52. Yamada, K.; Hikosaka, M.; Toda, A.; Yamazaki, S.; Tagashira, K. Macromolecules 2003, 36, 4802.
53. Zhao, Y.; Vaughan, A. S.; Sutton, S. J.; Swingler, S. G. Polymer 2001, 42, 6587.
54. Hoffman, J. D.; Weeks, J. J. J Res Natl Bur Stand 1962, A66, 13.
55. Marand, H.; Xu, J.; Srinivas, S. Macromolecules 1998, 31, 8219.
56. Xu, J.; Srinivas, S.; Marand, H.; Agarwal, P. Macromolecules 1998, 31, 8230.
57. Canetti, M.; De Chirico, A.; Audisio, G. J Appl Polym Sci 2004, 91, 1435.
58. Cheng, S. Z. D.; Janimak, J. J.; Zhang, A.; Cheng, H. N. Macromolecules 1990, 23, 298.
59. Lu, H.; Qiao, J.; Xu, Y.; Yang, Y. J Appl Polym Sci 2002, 85, 333.
60. Alamo, R. G.; Viers, B. D.; Mandelkern, L. Macromolecules 1995, 28, 3205.
61. Cazé, C.; Devaux, E.; Crespy, A.; Cavrot, J. P. Polymer 1997, 38, 497.
62. Zhang, Z.; Nawaby, A. V.; Day, M. J Polym Sci Part B: Polym Phys 2003, 41, 1518.
63. Khanna, Y. P. Polym Eng Sci 1990, 30, 1615.
64. Di Lorenzo, M. L.; Silvestre, C. Prog Polym Sci 1999, 24, 917.
65. Yamada, K.; Hikosaka, M.; Toda, A.; Yamazaki, S.; Tagashira, K. J Macromol Sci: Phys 2003, B42, 733.
66. Mandelkern, L.; Stack, G. M. Macromolecules 1984, 17, 871.
67. D'Orazio, L.; Mancarella, C.; Martuscelli, E.; Sticotti, G.; Cecchin, G. J Appl Polym Sci 1999, 72, 701.
68. Yazdami-Pedram, M.; Quijada, R.; López-Manchado, M. A. Macromol Mater Eng 2003, 288, 875.
69. Bedia, E. L.; Astrini, N.; Sudarisman, A.; Sumera, F.; Kashiro, Y. J Appl Polym Sci 2000, 78, 1200.
70. Yamaguchi, M.; Miyata, H.; Nitta, K.-h. J Appl Polym Sci 1996, 62, 87.